PET and MRI-guided focused ultrasound surgery for hypoxic-tissue ablation combined with radiotherapy in solid tumors

N.A. Koonce[1*], X. Chen[1,2], E.G. Moros[1,3], G. Shafirstein[4,5], P. Corry[1], R.J. Griffin[1]

[1]*Department of Radiation Oncology, University of Arkansas for Medical Sciences, USA*
[2]*Department of Radiation Oncology, Stanford University, USA*
[3]*Department of Radiation Oncology, Moffitt Cancer Center, Tampa, FL, USA*
[4]*Department of Otolaryngology, University of Arkansas for Medical Sciences, USA*
[5]*Department of Cell Stress Biology, Roswell Park Cancer Institute, USA*

► ***Original article***

**** Corresponding author:***
Dr. Nathan Koonce,
E-mail: *nakoonce@uams.edu*

Revised: June 2014
Accepted: Sept. 2014

Int. J. Radiat. Res., January 2015; 13(1): 1-12

ABSTRACT

Background: The rationale was to develop an ablation approach to destroy regions of tumor resistant to radiation and thus reduce the time required for whole tumor ablation, while improving overall tumor control after radiotherapy. ***Materials and Methods***: The system is composed of a micro positron emission tomography (mPET), 7T magnetic resonance imaging (MRI), and a customized MRI-compatible focused ultrasound applicator. 18F-fluoromisonidazole (18F-miso) radioactive tracer delineated hypoxic regions based on a threshold tumor/muscle activity ratio. 18F-miso PET/MRI fused images were used for targeting tumor hypoxic regions for focused ultrasound ablation. With MRI real-time temperature imaging guidance, PET-detected hypoxic regions of tumor could be selectively ablated to temperatures (T>55 ^{o}C). In vivo validation experiments were performed in SCK and 4T1 murine mammary carcinomas. In two tumor response assays, sequence dependence of combined radiotherapy and ablation was studied in the SCK tumor model. Tumor ablation was performed using a conductive probe or focused ultrasound and ionizing radiation administered in single doses of 15-20 Gy. ***Results***: Tumor growth was abolished when ablation was applied immediately AFTER radiation while interestingly; when ablation was administered immediately BEFORE radiation, there was no difference in observed growth delay compared to ablation or radiation alone. ***Conclusion***: PET and MRI guided focused ultrasound surgery (MRgFUS) of tumor hypoxic regions is feasible and will be potentially useful for preclinical studies using ultrasound, radiation or chemotherapy. This study suggests that radiation precedes ablative therapy to avoid unwanted stress response or additional hypoxia induced by the ablation, potentially confounding the improved response potential for combined therapy.

Keywords: *Hypoxia, thermal ablation, MRI/PET, radio-resistance.*

INTRODUCTION

A large volume of clinical and experimental data clearly demonstrates that tumor hypoxia remains a significant challenge for chemotherapy, photodynamic therapy and radiation therapy [1-5]. Hypoxia-related resistance is a major cause of treatment failures [6, 7]. Mild temperature hyperthermia (MTH, <43^{o}C) has been proposed to increase the overall oxygen concentration (i.e., pO_2) to improve tumor response and reduce

tumor recurrence [8-10]. Numerous efforts have also demonstrated the potential of developing small molecule drugs (e.g., bioreductive prodrugs) to directly kill hypoxic cells but few if any have made it to clinical use [11]. Rather than increasing tumor oxygenation using MTH or killing hypoxic cells using bioreductive prodrugs, we postulated that identification of the tumor hypoxia regions using imaging and subsequent thermal ablation of these regions to alleviate hypoxia-related resistance may synergize with conventional radiation or chemo- therapies. This may remove the need for ablation of the entire tumor- a prohibitive factor in many settings due to tumor size or location. To test this hypothesis, a hypoxia-directed ablation system for small animals was developed so that various comparative studies could be performed.

Compared with the available noninvasive methodologies to assess the oxygenation levels in soft tissue such as, ^{64}Cu-ATSM (diacetyl-bis (*N*8-methylthiosemicarbazone)) PET [12-15], ^{19}F MRI [16] and Blood-Oxygenation-Level-Dependent (BOLD) MRI [17, 18]; ^{18}F-fluoromisonidazole (^{18}F-miso) PET imaging was selected due to the wide availability and potential for quantitative analysis [19-22]. ATSM hypoxia imaging has been evaluated with several Cu-isotopes, ^{64}Cu showing the best signal/noise ratio. However, ^{64}Cu has a relatively longer half-life ($t_{1/2}$ = 12.7h) compared to ^{18}F ($t_{1/2}$ = 1.8h) and studies with ATSM-isotopes are often compared to ^{18}F-miso as the standard [23]. MRI trifluoroethoxy-misonidazole (TF-miso) imaging suffers from the necessity for large quantities (75mg/kg v 15μg) compared to ^{18}F-miso PET imaging [23] while BOLD MRI is an indirect measure of oxygenation as the technique measures deoxyhemoglobin, thus vascular volume and red blood cell density must be consistent per voxel for accurate measurements [24]. In contrast, ^{18}F-miso radiochemistry was first reported in 1986 and the mechanism of marking hypoxic cells is established in the literature [25].

As a thermal therapy method, Magnetic Resonance-guided Focused Ultrasound Surgery, MRgFUS, has become increasingly popular due to its high quality structural imaging, simultaneous temperature monitoring and noninvasive heat delivery. It has been clinically used to treat various diseases, for example; uterine fibroids [26-28], breast cancer [29], cervical cancer [30], liver cancer [31], and bone cancer including metastases [32]. For small animal studies, compact MRgFUS systems have been developed [33-35]. In this project, an MRI-compatible spherically-focused ultrasonic applicator was fabricated and installed in an animal immobilization cradle that can attach to a 7T MRI (Bruker) and a microPET (Siemens) scanner. While not optimal for image co-registration, we were able to use this approach for our preliminary proof-of-principle studies. In the future, an integrated PET-MRI scanner for simultaneous imaging will advance this research approach due to a significant reduction in the potential misplacement of patient's during transfer from PET to MRI [36, 37].

Here, we report on the development and performance evaluation of our preclinical PET and MR-guided focused ultrasound (MRgFUS) surgery system and the general usefulness of a combined radiation and ablation treatment approach for advanced solid tumors. The significance of potential applications, limitations, combined therapy and future development of this system are discussed.

MATERIALS AND METHODS

Experimental protocol for PET and MRgFUS

The experimental protocol of PET and MRI-guided hypoxia-directed ablation in mouse tumors was approved by the University of Arkansas for Medical Sciences (UAMS) Institutional Animal Care and Use Committee (IACUC). As illustrated in figure 1, it includes: (1) injection of the ^{18}F-miso agent, (2) identification of hypoxic areas with PET imaging and MR structural imaging, and (3) focused ultrasound ablation of hypoxic targets guided by real-time MR temperature imaging. Mouse breast tumor cell lines (SCK or 4T1) were implanted subcutaneously into the right hind limb of A/J or balb/c conventional mice as described previously and shown in figure 1 [38, 39]. Six tumor bearing (table 1) were used for the PET/MRgFUS study when the

tumors grew to approximately 1 cm in diameter. The mice were kept under general anesthesia during imaging and ablation by breathing 1-1.5% isoflurane balanced with air. To reduce the motion, the animal breathing rate was closely monitored and the flow rate of isoflurane air was manually controlled.

Identification of tumor hypoxic regions

The ^{18}F-miso tracer was produced on-site as described previously with a Siemens/CTI medical cyclotron (3D Imaging, Little Rock, AR) and transferred to the small animal imaging suites [40]. The ^{18}F-miso agent with 1.05 ± 0.11 mCi (mean ± standard deviation) was assayed by a dose calibrator (Capintec CRC-15W) and immediately injected intravenously (i.v.) via the tail vein (as indicated in figure 1 and table 1). The mouse, focused ultrasound transducer, breathing monitor and anesthesia tube were set up and secured in an animal immobilization cradle. MicroPET three-dimensional PET images were acquired 90-125 minutes after tracer uptake and images reconstructed requiring approximately 30 minutes for the initial microPET procedure and image processing [41]. The biodistribution of ^{18}F-miso tracer was analyzed using the microPET analysis software (ASI Pro VM ™). Attenuation and scatter are corrected by a normalization scan and image reconstruction was performed using a 2D ordered-subset expectation maximization (OSEM2D) algorithm. Multi-slice transverse PET images of the tumor region were exported to an independent computer for registration with T2-weighted images from the subsequent MRI anatomical imaging study. The measured isotope uptake in the tumor and the left healthy thigh (as a reference) were used to calculate the tumor-muscle (T/M) activity ratio pixel by pixel. In this study, the hypoxic regions were characterized and delineated with the criteria of T/M > 1.2 [42, 43].

MR structural and temperature imaging

Following PET scanning, the cradle with the setup intact was transferred to a 7T MRI (PharmaScan, Bruker). The sequence of Rapid Acquisition with Refocused Echoes (RARE) T2-weighted imaging (table 2) was conducted. By aligning the PET images with the high resolution MR T2-weighted structural images, the ^{18}F-miso-detected hypoxic areas can be overlaid on the MRI T2-w images to serve as targets for MRgFUS

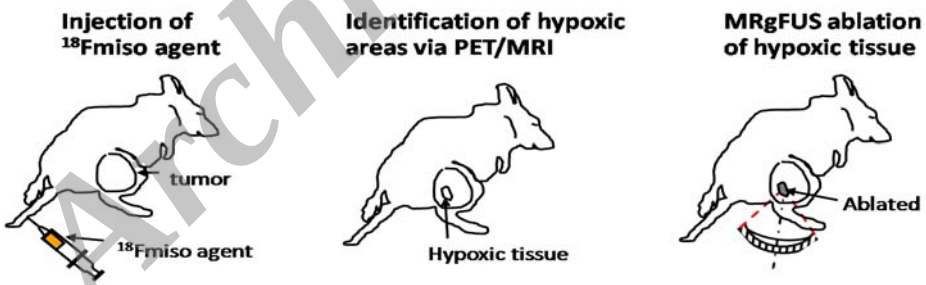

Figure 1. Three basic steps of PET/MRI-guided FUS hypoxic-tissue ablation.

Table 1. Record of ^{18}F-miso isotope uptake by tumor bearing mice.

Tumor model	*Tumor type*	*Tumor size (cm i.d.)*	*Mouse weight (g)*	*Activity (mCi)*	*Tumor initial temperature (°C)*	*Uptake time (min)*
1	SCK	1.0	21	0.89	32.4	90
2	SCK	1.9	17	1.12	35.1	100
3	4T1	1.2	22	1.05	30.7	102
4	4T1	1.1	20	1.20	31.2	120
5	4T1	1.7	18	1.08	32.6	125
6*	4T1	1.2	17	0.97	34.2	95

Note: the sixth mouse is used as the example in Figure 7 to present MR temperature maps during FUS ablation.

ablation. A user interface (Visual C++) was developed on an independent computer, into which the PET and MRI data could be imported from the MRI and microPET workstations respectively and processed. The online MR temperature imaging during the FUS heating was done using a Fast Low Angle Shot (FLASH, table 2) MRI sequence [44]. Based on the Proton resonance frequency (PRF) – shifted scheme, three slices of temperature images were computed as a guidance to modulate and terminate the FUS heating.

MRI-compatible FUS applicator

A non-magnetic single spherically-focused ultrasound applicator was devised based on the parameters obtained from numerical simulations. As illustrated in figure 2-a, the aperture size (38 mm in diameter) could produce sufficient acoustic power (resonant frequency 2.25MHz) for ablations. It was able to fit into the animal cradle and the bore (60 mm in diameter) of a 7.0 T Bruker MRI scanner. The focal length of the spherical shell was chosen to be 50 mm, ensuring the ability to ablate at various depths. A piezoelectric ceramic transducer (Boston Piezo-Optics, Inc., Boston, MA) was secured in an acrylic frame with air backing and sealed using silicone to maintain watertight integrity. An acrylic water filled housing was attached in the front of the transducer for acoustic coupling between the transducer and the tumor; it was conical to assist in aiming the acoustic focus on the target.

The relative acoustic pressure distribution of this transducer was measured in a degassed water tank; the relative power distribution (i.e., the squared acoustic pressure) is shown in figure 2-b. A needle hydrophone (Model Dapco #NP10-1, active diameter = 0.2 mm) was moved using a computer-controlled three-axes scanning system (NF90 series stepping motor controller, Velmex inc.) in a rectangular focal plane (40×40 mm). The applied sonication for these measurements was with an electrical input power of 1.0 W at a frequency of 2.25 MHz. The scanning step size was set close to the diameter of the hydrophone, 0.2 mm along the x, y and z directions. 15 W of acoustic power was supplied on the transducer surface, which produced 3.63 MPa at the center. The heating performance of this applicator has been verified via ablations in gel phantom, *ex-vivo* and *in-vivo* mouse tumors [33].

Table 2. The imaging parameters of ^{18}F-miso PET and MR imaging.

Imaging modalities	Function	Parameters
PET	Hypoxia	Isotope, ^{18}fluromisonidazole, dose = 1.0±0.1 mCi/mouse, injected i.v. 120 minutes uptake
MRI sequences T2 RARE	Structure	TR/TE = 2500/33, NSA = 3, Flip angle=180º, Number of slice = 9, FOV = 40 * 40 mm, Matrix = 256x256, Resolution = 0.16*0.16 mm
MRI FLASH	Temperature	TR/TE = 37/3.4, FOV = 45*45 mm, Slice = 3, Resol = 0.18*0.35, Matrix = 256*128

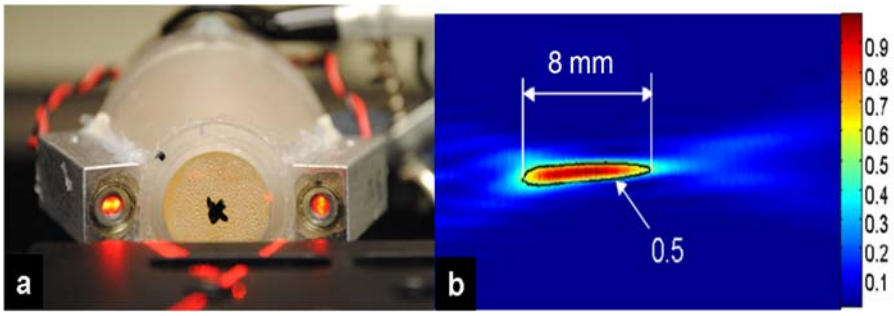

Figure 2. Non-magnetic focused ultrasound device. (a) The single spherically-focused ultrasound applicator with a laser localizer indicating the focus position, (b) the measured sound pressure squared (power).

Ablation of tumor hypoxic regions

Prior to the ablation, the mouse tumors were shaved to allow for acoustic coupling with the ultrasound field produced by FUS sonication. The initial tumor temperature T_0 was measured with a subcutaneously-inserted thermocouple. Based on T_0, a sequence of MR temperature images acquired during ablation was used to create a temperature map using the MR-measured temperature changes. As shown in figure 3, once a hypoxic target was determined, we performed a FUS preview heating prior to the FUS ablation. The preview heating was short and mild (e.g. in this study, 10W acoustic power for 2s, the peak temperature <43°C) so that the actual position of the focus could be visualized by a MR temperature image while the tissue was not thermally damaged. Based on the distance between the actual and planned position of the focus, we repositioned the FUS applicator until the ultrasound focus matched the planned spot. The hypoxic regions were then ablated using the MRgFUS method, in which the heating was manually modulated based on the simultaneous real-time MR temperature monitoring. In some cases, animal motion occurred due to muscle contraction, inconsistent isoflurane supply, or reaction to noise coming from the MRI gradient magnets. If severe motion occurred, repositioning of the FUS applicator and registration between PET and MR images was performed.

Tumor growth delay assay and combined-modality treatment

In the tumor growth delay study, two separate experiments were performed using two ablation techniques. In both studies, SCK tumor bearing A/J mice were randomly assigned to each group (n=3-6) when tumor volume reached approximately 250 mm^3. In the first study, groups were as follows: control (untreated), HIFU ablation, 15 Gy ionizing radiation, or HIFU ablation immediately followed by 15 Gy ionizing radiation. HIFU ablation was performed as described previously, were temperature within the tumor reached >50C [45]. Only partial tumor ablation was performed in order to study the effects when combined with radiotherapy. Radiotherapy was administered using the Small Animal Conformal Radiation Research System (SACRRS) at a dose rate of 1.92 Gy/min at 225 kV and 13 mA [46, 47] under isoflurane anesthesia.

In the second study, groups were as follows: control (untreated), conductive ablation (CITT)

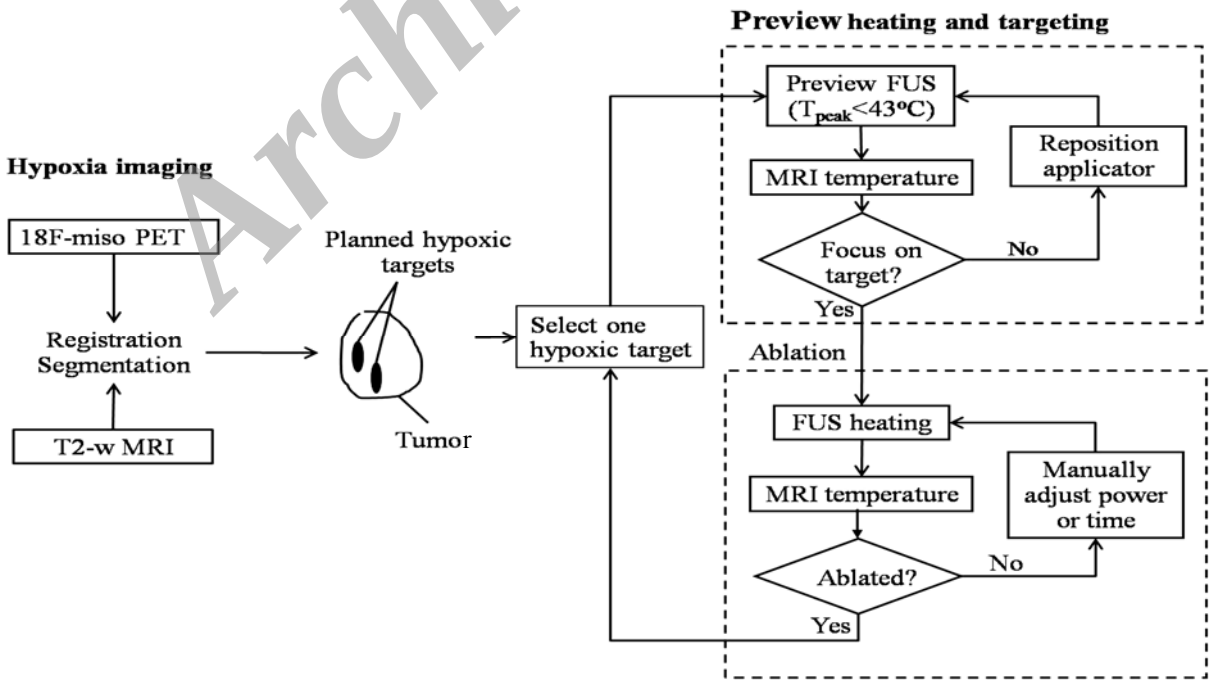

Figure 3. Protocol of PET/MRI-guided hypoxic-tissue ablation.

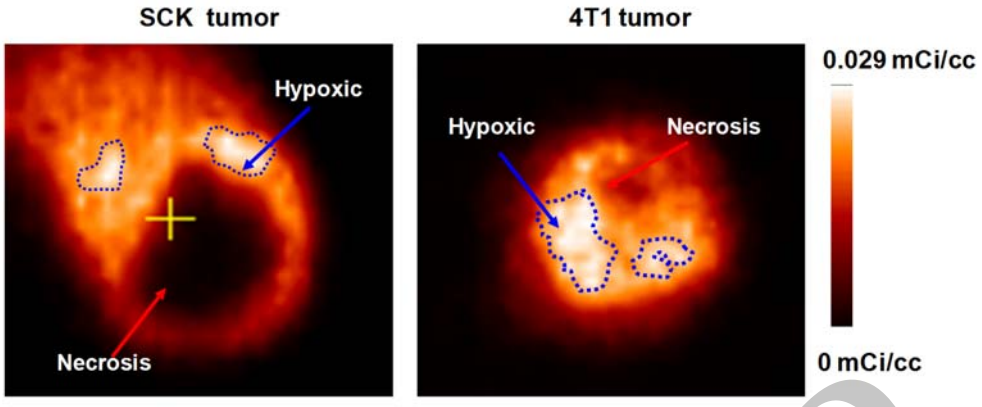

Figure 4. Representative ^{18}F-miso mPET images of 4T1 and SCK mammary carcinomas. Compared with 4T1 tumors, the SCK tumors typically demonstrated a larger necrotic, non-perfused region with similar amounts of 18F-miso uptake in the viable regions.

alone, 20 Gy ionizing radiation or 20 Gy ionizing radiation immediately followed by CITT ablation. CITT ablation was used as the ablation modality for proof of principle in these studies due to the relative ease of partially ablating the central portion of a larger group of tumors in a relatively consistent fashion. In brief, CITT ablation was performed using a custom laser-heated stainless steel ablation probe as described previously [39]. After inserting into the center of the tumor (approximately 5 mm deep) a temperature range of 70-80C was maintained at the ablative probe tip for 5 minutes. Radiotherapy was performed as a single treatment dose of 20Gy using a Faxitron X-ray cabinet system (CP-160, Faxitron X-Ray Corp., Wheeling, IL) at a dose rate of 1.079Gy/min (150 kVp and 6.6 mA) under ketamine/xylazine anesthesia.

RESULTS

PET hypoxia imaging of mouse tumors

In all instances, three-dimensional ^{18}F-miso mPET images of mouse tumors with i.v. injection of 1 mCi per mouse and 90-125 minutes of uptake clearly distinguished regions of hypoxic, necrotic, and oxygenated volumes in a solid tumor. In figure 4, the uptake of ^{18}F-miso in SCK and 4T1 tumors is demonstrated using identical scales, from 0 to 29 µCi/cc. The contours of T/M ratio with a value of 1.2 are delineated. The central dark area was determined to be necrotic regions typical of these tumor types, in which the isotope did not distribute due to lack of blood supply.

3D hypoxic volumes in mouse tumors

In all six animals, the mice were kept immobile under anesthesia resulting in motion artifacts being negligible, allowing PET and MR images to be aligned without using other registration algorithms. In figure 5, an example of multi-slice MRI RARE T2-weighted anatomical images (left column) and ^{18}F-miso PET images (middle column) of a 4T1 tumor were complementary to one another and provide precise 3D location of the hypoxic regions (the right column). The volumes of the PET-detected hypoxic regions in tumors of all six mice were estimated from the images by outlining the regions of interest with tumor/muscle (T/M) ratio > 1.2 and are plotted in figure 6. The MR temperature imaging-guided preview heating worked effectively in all instances to properly align the focus on the hypoxic target. The ablations were successfully done with pulsed FUS power (2.25MHz, 15 Watts), an example of which is shown in figure 7. Sequences of MR temperature maps were acquired continuously to describe the dynamic temperature distributions through the ablation. The maximum temperature was approximately 70^{o} C. The MRI temperature imaging and the focused ultrasound heating were performed simultaneously and no significant interference was detected.

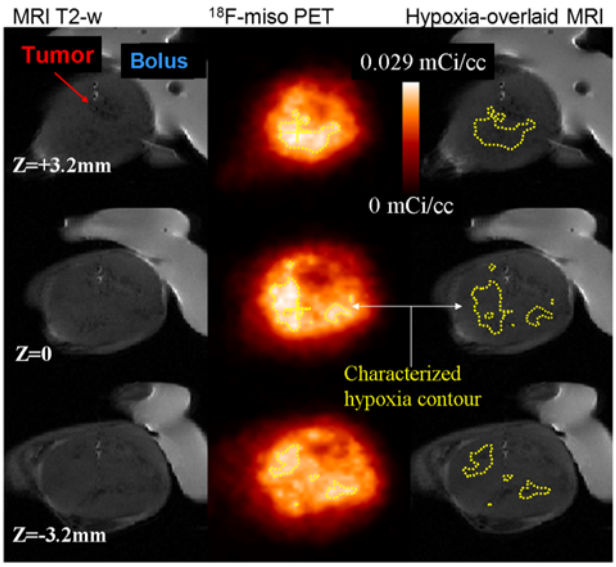

Figure 5. Registration of MRI T2-weighted and ^{18}F-miso PET images of three transverse slices of a 4T1 tumor. The hypoxic areas characterized by contours of tumor/muscle (T/M) ratio >1.2. The water bolus used is shown in the MRI T2-weighted images but not in the PET images.

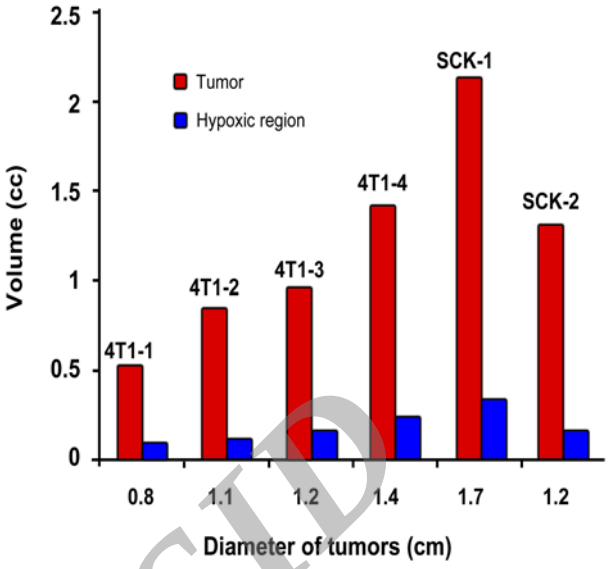

Figure 6. Tumor volumes and the extent of ^{18}F-miso PET identified hypoxic regions. Horizontal axis represents the mean diameter of the tumor.

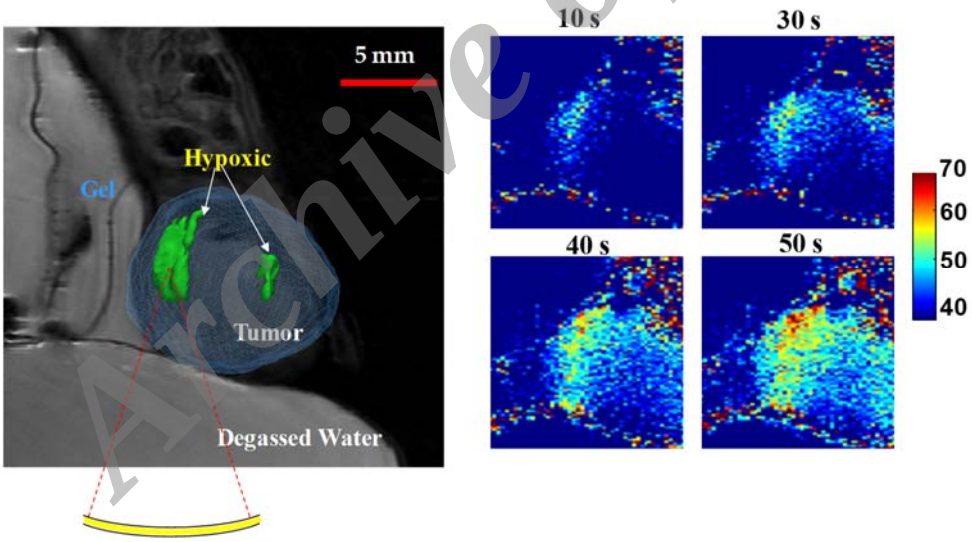

Figure 7. MRgFUS ablation of hypoxic regions in a tumor implanted in right hind limb of a mouse. A) T2-weighted image overlapped with 3-D hypoxic regions that were reconstructed based on PET images; B) a time sequence of temperature maps during ablation.

Combined radiotherapy and ablation enhances tumor growth delay only when ablation follows radiation

In two separate studies we combined radiotherapy with partial tumor ablation, simulating possible sequences of treatment if hypoxic targeted ablation were executed in future multi-functional therapy suites. In the first study, partial ablation using HIFU, 15Gy irradiation, and ablation immediately followed by 15 Gy irradiation all resulted in modest but indistinguishable increases in tumor growth delay. A greater than 3-fold increase in tumor volume was observed in all treatment groups by day 12

(the end of the study), compared to a 3.8-fold change observed in the control group by day 7, figure 8a. In the second study, partial ablation using conductive heating resulted in a tumor growth delay to reach four times the starting volume of 1.3-fold compared to control (day 6 v. day 8). By day 14 after treatment, the average tumor growth in the radiation alone and ablation alone progressed past 3-fold the starting volume. In contrast, the average tumor volume in tumors treated with radiation immediately followed by ablation regressed to below the average starting volume by day 14, figure 8b- in essence a full inhibition of tumor re-growth over this time frame.

DISCUSSION

The prognostic importance and treatment resistance features ascribed to hypoxia in tumor tissue makes tumor hypoxia a high priority target for cancer treatment and diagnostic evaluation [48]. The current project aimed to develop an ^{18}F-miso PET and MRI guided FUS system to selectively ablate identified tumor hypoxic regions and test sequence dependence when combined with a conventional treatment such as radiotherapy. Following the experimental protocol (figure 1 and 3), the effectiveness of this system using PET hypoxia imaging (figure 4), alignment of PET and MRI T2-w images (figure 5 and 6), and the performance of MRI temperature imaging and FUS heating were tested *in vivo* using two models of breast carcinoma in tumor bearing mice (figure 7).

The measurement of tumor hypoxia using ^{18}F-miso PET has been previously validated using a polarographic needle electrode system (49). The tumor pO_2 measured by the polarographic needle correlated with the positron emitter ^{18}F-miso agent in tumor tissue in terms of tumor-to-muscle ratio ($FMISO_{T/M\ 2h}$). In our current work, the $FMISO_{T/M\ 2h}$ that corresponded to 60% of the pO_2 readings < 5.0 mmHg was used as the nominal threshold to characterize the most hypoxic tumor regions (figure 4 and 5). A potential artifact in our results is the effect of sedation on tumor oxygenation. Measurements of tumor pO_2 under isoflurane anesthesia [50] have revealed that as animals are anesthetized by the inhalation of isoflurane balanced by air, the tumor pO_2 value will decrease rapidly within 1–2 min and remains stable thereafter. Careful attention to maintaining physiological blood chemistry while performing pre-clinical experiments will need to be considered in future experiments. However, this may or may not have bearing on clinical studies, as patients are not normally sedated during PET/MRI scans- yet

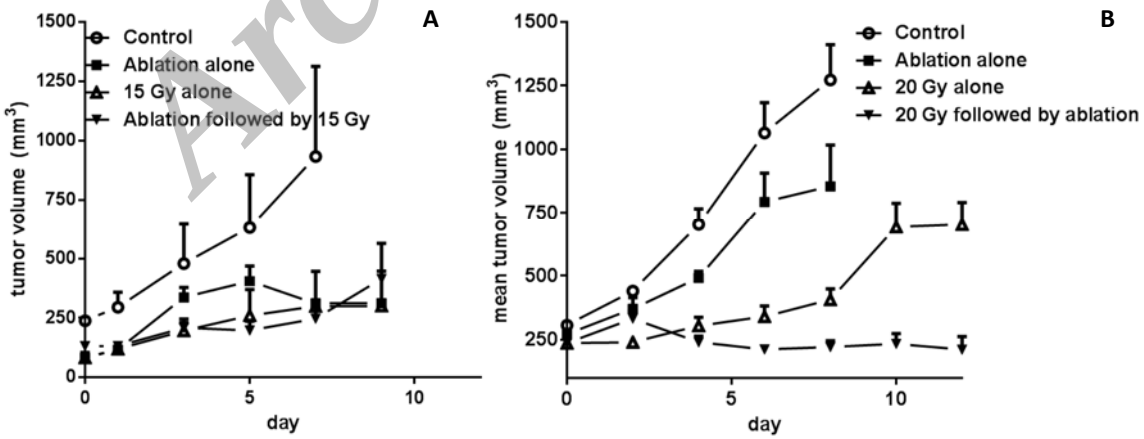

Figure 8. Tumor growth delay of SCK mammary carcinomas following treatment regimens of ablation, radiation and combined therapy. Effect of treatment on tumor growth was monitored using caliper measurements and plotted as means ± SE. A) Tumors were treated with either HIFU ablation, 15 Gy alone or combined therapy. n= 4-6 tumors/group B) Tumors were treated with conductive probe ablation, 20 Gy alone or combined therapy. n= 3-5 tumors/group.

they may be when ablative procedures are administered.

The spatial resolution of PET hypoxia imaging is limited by many factors such as detector size, photon non-colinearity, and positron range [51]. In our studies, the microPET (FOCUS, Siemens) system used for animal studies with ^{18}F-miso tracer has the spatial resolution of nearly 1.4 mm FWHM (full width at half maximum). In other words, the uncertainty of ^{18}F-miso PET-detected hypoxic contours (figure 4 and 5) was reasonable for this work, compared to the pixel size of MRI T2-w imaging (1.6 mm, figure 5). This is an important issue to keep in mind during clinical development of this approach since resolution may decrease and therefore the ablation volumes to target may become more difficult to determine. Albeit, the method described is presumably for larger bulky tumors, where ablative margins of hypoxic regions are within the tumor volume and can likely be expanded to ensure complete ablation of these regions assuming no proximal critical anatomy is involved. Ablative margins for whole tumor ablation are in the 0.5-1cm range and thus targeting potential hypoxia in tumor periphery will likely not be limited either [52].

In our current setup, the 7T MRI scanner can introduce adequate signal-to-noise ratio (SNR) but has a higher risk of phase wrapping artifacts in PRF shifted temperature maps. To achieve wrap-free phase changes, i.e., to limit that the phase variation in the range from zero to π, the maximum temperature change in tumor between two acquisitions has to be controlled (e.g., $\Delta T_{max} < 50^{o}C$ in this study) by carefully modulating the FUS heating. An unwrapping algorithm will be necessary otherwise, which would be best avoided due to its time-consuming nature and lack of ability for direct online analysis. Overall, interference was found to be of no significance within the parameters used in this study.

The potential development of tumor hypoxia post-MRgFUS treatment may occur after this treatment approach, which could cause unwanted additional radiation resistance. The MRgFUS ablation will create a well-demarcated zone of vascular collapse in the hypoxic target that is irreversibly ablated and destined to become necrotic. In addition, oxygenation in the surrounding tissue may temporarily increase after exposure to hyperthermic temperatures such as those expected at the edge of the ablation zone, based on our previous data [53-55]. This may be critical, as areas of intermediate hypoxia possibly not ablated given the ^{18}F-miso T/M ratio thresholds used may be responsible for failure of treatment response to radiotherapy or other therapies [56]. Previous work by our group indicates reoxygenation of the surrounding viable tumor tissue persist at least 72h post partial tumor ablation, suggesting radio sensitization of this area may occur- yet defining the most effective interval between ablation and radiation could prove tricky for easy adoption into clinical practice [39]. Indeed, our tumor response studies (figure 8) suggest that there may be good logic to applying the hypoxic-targeted ablation after radiotherapy is administered. Although areas of hypoxia were not selectively ablated in the breast tumor model studied, there was a distinctive sequence dependence of treatments applied. Irradiation followed by ablation was clearly the most effective treatment sequence tested. The cause of the sequence dependent anti-tumor response may be because radiation at a high dose of 20 Gy easily kills all of the oxic cells, and the following ablation preferentially kills regions where perfusion is limited and hypoxia may be present. Conversely, when ablation precedes radiation, there may be additional hypoxia and stress response induced in the tissue surrounding the ablation zone which blunts the radio sensitivity of this tissue and results in negligible combined treatment improvement. More clearly understanding these variables may allow clinicians to better tailor a combined treatment approach of radiation and hypoxia-targeted HIFU as illustrated in this study.

The use of thermal ablation is typically hampered when trying to fully ablate large tumors because of long treatment sessions and potential to miss small volumes of tumor in the mass. Because the described new method will involve significantly shortened ablation treatments to only a portion of the tumor and

potentially improved radiation or chemotherapy response by the remainder of the tumor, FUS therapy may be adopted into treatment regimens for a wider range of solid tumors. This is the first report to our knowledge to study the acute sequence dependence of thermal ablation and combined radiation therapy applied on the same day. Further experiments to understand the sequence dependence of selective, hypoxia targeted thermal ablation and radiation appear attractive as MRgFUS and other thermal ablative techniques expand their role in cancer therapy.

In summary, irreversible destruction of tumor hypoxic tissue and poorly perfused tissue in general can potentially reduce hypoxic radioprotection and improve tumor control when properly combined with radiotherapy. This idea of treating with complementary therapies, radiotherapy and thermal ablation, with reciprocal zones of efficacy is attractive and some clinical studies have already suggested that the approach has potential [57]. MRI-guided ablation of hypoxic regions of tumors as part of definitive therapy in combination with chemo radiation therapy could become a new clinical indication for MRgFUS.

ACKNOWLEDGEMENTS

This research was supported by a grant from the Focused Ultrasound Surgery Foundation (FUSF), NIH/NCI grant CA44114, and the Arkansas Breast Cancer Research Program.

Conflicts of interest: *none to declare.*

REFERENCES

1. Yotnda P, Wu D, Swanson, AM (2010) Hypoxic tumors and their effect on immune cells and cancer therapy. *Methods Mol Biol,* ***651:*** *1-29.*
2. Wouters A, Pauwels B, Lardon F, Vermorken JB (2007) Review: implications of in-vitro research on the effect of radiotherapy and chemotherapy under hypoxic conditions. *Oncologist,* ***12(6):*** *690-712.*
3. Harrison LB, Chadha M, Hill RJ, Hu K, Shasha D (2002) Impact of tumor hypoxia and anemia on radiation therapy outcomes. *Oncologist,* ***7(6):*** *492-508.*
4. Busch TM, Hahn SM, Evans SM, Koch CJ (2000) Depletion of tumor oxygenation during photodynamic therapy: detection by the hypoxia marker EF3 [2-(2-nitroimidazol-1[H]-yl)-N-(3,3,3-trifluoropropyl)acetamide]. *Cancer Res,* ***60 (10):*** *2636-42.*
5. Brown JM, Diehn M, Loo BW (2010) Stereotactic ablative radiotherapy should be combined with a hypoxic cell radiosensitizer. *Int J Radiat Oncol Biol Phys,* ***78(2):*** *323-7.*
6. Rofstad EK, Sundfor K, Lyng H, Trope CG (2000) Hypoxia-induced treatment failure in advanced squamous cell carcinoma of the uterine cervix is primarily due to hypoxia-induced radiation resistance rather than hypoxia-induced metastasis. *Br J Cancer,* ***83(3):*** *354-9.*
7. Bourke VA, Zhao D, Gilio J, Chang CH, Jiang L, *et al.* (2007) Correlation of radiation response with tumor oxygenation in the Dunning prostate R3327-AT1 tumor. *Int J Radiat Oncol Biol Phys,* ***67(4):*** *1179-86.*
8. Griffin RJ and Corry PM (2009) Commentary on classic paper in hyperthermic oncology 'Tumour oxygenation is increased by hyperthermia at mild temperatures' by CW Song et al., 1996. *Int J Hyperthermia,* ***25(2):*** *96-8.*
9. Song CW, Shakil A, Osborn JL, Iwata K (2009) Tumour oxygenation is increased by hyperthermia at mild temperatures. 1996. *Int J Hyperthermia,* ***25(2):*** *91-5.*
10. Thrall DE, Larue SM, Pruitt AF, Case B, Dewhirst MW (2006) Changes in tumour oxygenation during fractionated hyperthermia and radiation therapy in spontaneous canine sarcomas. *Int J Hyperthermia,* ***22(5):*** *365-73.*
11. Wilson WR and Hay MP (2011) Targeting hypoxia in cancer therapy. *Nat Rev Cancer,* ***11(6):*** *393-410.*
12. O'Donoghue JA, Zanzonico P, Pugachev A, Wen B, Smith-Jones P et al. (2005) Assessment of regional tumor hypoxia using 18F-fluoromisonidazole and 64Cu(II)-diacetyl-bis(N4-methylthiosemicarbazone) positron emission tomography: Comparative study featuring microPET imaging, Po2 probe measurement, autoradiography, and fluorescent microscopy in the R3327-AT and FaDu rat tumor models. *Int J Radiat Oncol Biol Phys,* ***61(5):*** *1493-502.*
13. Lewis JS, McCarthy DW, McCarthy TJ, Fujibayashi Y, Welch MJ (1999) Evaluation of 64Cu-ATSM in-vitro and in-vivo in a hypoxic tumor model. *J Nucl Med,* ***40(1):*** *177-83.*
14. Yuan H, Schroeder T, Bowsher JE, Hedlund LW, Wong T et al. (2006) Intertumoral differences in hypoxia selectivity of the PET imaging agent 64Cu(II)-diacetyl-bis(N4-methylthiosemicarbazone). *J Nucl Med,* ***47(6):*** *989-98.*
15. Wood KA, Wong WL, Saunders MI (2008) [(64)Cu]diacetyl-bis(N(4)-methyl-thiosemicarbazone) - a radiotracer for tumor hypoxia. *Nucl Med Biol,* ***35(4):*** *p. 393-400.*
16. Diepart C, Magat J, Jordan BF, Gallez B (2010) In-vivo mapping of tumor oxygen consumption using (19)F MRI relaxometry. *NMR Biomed,* ***24:*** *458–463*
17. Ogawa S, LeeTM, Kay AR, Tank DW (1990) Brain magnetic resonance imaging with contrast dependent on blood oxygenation. *Proc Natl Acad Sci USA,* ***87(24):*** *9868-72.*
18. Kamba M, Sung YW, Ogawa S (2007) Alteration of blood oxygenation level-dependent signaling by local circulatory condition. *J Magn Reson Imaging,* ***26(6):*** *1506-13.*

19. Rojas S, Herance JR, Abad S, Jimenez X, Pareto D *et al.* (2010) Evaluation of Hypoxic Tissue Dynamics with (18)F-FMISO PET in a Rat Model of Permanent Cerebral Ischemia. *Mol Imaging Biol,* ***13:*** *558-564.*
20. Rajendran JG, WilsonDC, Conrad EU, Peterson LM, Bruckner JD et al. (2003) [(18)F]FMISO and [(18)F]FDG PET imaging in soft tissue sarcomas: correlation of hypoxia, metabolism and VEGF expression. *Eur J Nucl Med Mol Imaging,* ***30(5):*** *695-704.*
21. Liu RS, Chou TK, Chang CH, Wu CY, Chang CW et al. (2009) Biodistribution, pharmacokinetics and PET imaging of [(18)F]FMISO, [(18)F]FDG and [(18)F]FAc in a sarcoma- and inflammation-bearing mouse model. *Nucl Med Biol,* ***36(3):*** *305-12.*
22. Dence CS, Ponde DE, Welch MJ, Lewis JS (2008) Autoradiographic and small-animal PET comparisons between F-FMISO, (18)F-FDG, (18)F-FLT and the hypoxic selective (64)Cu-ATSM in a rodent model of cancer. *Nucl Med Biol,* ***35(6):*** *713-20.*
23. Kurihara H, Honda N, Kono Y, Arai Y (2012) Radiolabelled agents for PET imaging of tumor hypoxia. *Curr Med Chem,* ***19(20):*** *3282-9.*
24. Fine LG and Dharmakumar R (2012) Limitations of BOLD-MRI for assessment of hypoxia in chronically diseased human kidneys. *Kidney Int,* ***82(8):*** *934-935.*
25. Jerabek PA, Patrick TB, Kilbourn MR, Dischino DD, Welch MJ (1986) Synthesis and biodistribution of 18F-labeled fluoronitroimidazoles: potential in-vivo markers of hypoxic tissue. *Int J Rad Appl Instrum A,* ***37(7):*** *599-605.*
26. Taran FA, Tempany CM, Regan L, Inbar Y, Revel A *et al.* (2009) Magnetic resonance-guided focused ultrasound (MRgFUS) compared with abdominal hysterectomy for treatment of uterine leiomyomas. *Ultrasound Obstet Gynecol,* ***34(5):*** *572-8.*
27. Pilatou MC, Stewart EA, Maier SE, Fennessy FM, Hynynen K et al. (2009) MRI-based thermal dosimetry and diffusion -weighted imaging of MRI-guided focused ultrasound thermal ablation of uterine fibroids. *J Magn Reson Imaging,* ***29(2):*** *404-11.*
28. Gedroyc WM (2009) MRgFUS: a sound approach to fibroid therapy. *Ultrasound Obstet Gynecol,* ***34(5):*** *494-6.*
29. Schmitz AC, van den BoschMA, Rieke V, Dirbas FM, Butts Pauly K et al. (2009) 3.0-T MR-guided focused ultrasound for preoperative localization of nonpalpable breast lesions: an initial experimental ex vivo study. *J Magn Reson Imaging,* ***30(4):*** *884-9.*
30. Machtinger R, Inbar Y, Ben-Baruch G, Korach J, Rabinovici J (2008) MRgFUS for pain relief as palliative treatment in recurrent cervical carcinoma: a case report. *Gynecol Oncol,* ***108(1):*** *241-3.*
31. Quesson B, Merle M, Kohler MO, Mougenot C, Roujol S *et al.* (2010) A method for MRI guidance of intercostal high intensity focused ultrasound ablation in the liver. *Med Phys,* ***37(6):*** *2533-40.*
32. Catane R, Beck A, Inbar Y, Rabin T, Shabshin N *et al.* (2007) MR-guided focused ultrasound surgery (MRgFUS) for the palliation of pain in patients with bone metastases --preliminary clinical experience. *Ann Oncol,* ***18(1):*** *163-7.*
33. Chen X, Novak P, Benson D, Webber J, Hennings L *et al.* (2011) An alternating focused ultrasound system for thermal therapy studies in small animals. *Med Phys,* ***38(4):*** *1877-1887.*
34. Chopra R, Curiel L, Staruch R, Morrison L, Hynynen K (2009) An MRI-compatible system for focused ultrasound experiments in small animal models. *Med Phys,* ***36(5):*** *1867-74.*
35. Larrat B, Pernot M, Aubry JF, Dervishi E, Sinkus R *et al.* (2010) MR-guided transcranial brain HIFU in small animal models. *Phys Med Biol,* ***55(2):*** *365-88.*
36. Buchbender C, Heusner TA, TC Lauenstein, Bockisch A, Antoch G (2012) Oncologic PET/MRI, Part 1: Tumors of the Brain, Head and Neck, Chest, Abdomen, and Pelvis. *Journal of Nuclear Medicine,* ***53(6):*** *928-938.*
37. Buchbender C, Heusner TA, Lauenstein TC, Bockisch A, Antoch G (2012) Oncologic PET/MRI, Part 2: Bone Tumors, Soft-Tissue Tumors, Melanoma, and Lymphoma. *Journal of Nuclear Medicine,* ***53(8):*** *1244-1252.*
38. Shao J, Griffin RJ, Galanzha EI, Kim JW, Koonce N *et al.* (2013) Photothermal nanodrugs: potential of TNF-gold nanospheres for cancer theranostics. Sci Rep, 3: 1293.
39. Przybyla BD, Shafirstein G, Koonce NA, Webber JS, Griffin RJ (2012) Conductive thermal ablation of 4T1 murine breast carcinoma reduces severe hypoxia in surviving tumour. *Int J Hyperthermia,* ***28(2):*** *156-62.*
40. Lim JL and Berridge MS (1993) An efficient radiosynthesis of [18F]fluoromisonidazole. *Appl Radiat Isot,* ***44(8):*** *1085-91.*
41. *Rajendran JG, Schwartz DL*, O'Sullivan J, Peterson LM, Ng P et al. (2006) Tumor Hypoxia Imaging with [F-18] Fluoromisonidazole Positron Emission Tomography in Head and Neck Cancer. *Clinical Cancer Research,* ***12(18):*** *5435-5441.*
42. Lee ST and Scott AM (2007) Hypoxia positron emission tomography imaging with 18f-fluoromisonidazole. *Semin Nucl Med,* ***37(6):*** *451-61.*
43. Yeh SH, Liu RS, Wu LC, Yang DJ, Yen SH et al. (1996) Fluorine-18 fluoromisonidazole tumour to muscle retention ratio for the detection of hypoxia in nasopharyngeal carcinoma. *Eur J Nucl Med,* ***23(10):*** *1378-83.*
44. Haacke EM (1999) Magnetic resonance imaging : physical principles and sequence design., New York: J. Wiley & Sons. xxvii, 914.
45. Novák P, Jamshidi-Parsian A, Benson DG, Webber JS, Moros EG et al. (2009) Multi-Angle Switched HIFU: A New Ultrasound Device for Controlled Non-Invasive Induction of Small Spherical Ablation Zones—Simulation and Ex-Vivo Results. AIP Conference Proceedings, 1113(1): p. 387 -391.
46. Asur RS, Sharma S, Chang CW, Penagaricano J, Kommuru IM *et al.* (2012) Spatially Fractionated Radiation Induces Cytotoxicity and Changes in Gene Expression in Bystander and Radiation Adjacent Murine Carcinoma Cells. Radiation Research, 177(6): 751-765.
47. Sridharan V, Aykin-Burns N, Tripathi P, Krager KJ, Sharma SK *et al.* (2014) Radiation-Induced Alterations in Mitochondria of the Rat Heart. *Radiation Research,* ***181(3):*** *324-334.*

48. Horsman MR, Mortensen LS, Petersen JB, Busk M, Overgaard J (2012) Imaging hypoxia to improve radiotherapy outcome. *Nat Rev Clin Oncol,* ***9(12):*** *674-87.*
49. Gagel B, Reinartz P, DiMartino E, Zimny M, Pinkawa M et al. (2004) pO2 Polarography Versus Positron Emission Tomography ([18F] Fluoromisonidazole, [18F]-2-Fluoro-2'-Deoxyglucose). *Strahlentherapie und Onkologie,* ***180(10):*** *616-622.*
50. Wen B, Urano M, O'Donoghue JA, Ling CC (2006) Measurements of partial oxygen pressure pO2 using the OxyLite system in R3327-AT tumors under isoflurane anesthesia. *Radiat Res,* ***166(3):*** *512-8.*
51. Budinger TF (1998) PET instrumentation: what are the limits? *Semin Nucl Med,* ***28(3):*** *247-67.*
52. Goldberg SN, Grassi CJ, Cardella JF, Charboneau JW, Dodd Iii GD et al. (2005) Image-guided Tumor Ablation: Standardization of Terminology and Reporting Criteria. *Journal of Vascular and Interventional Radiology,* ***16(6):*** *765-778.*
53. Griffin RJ, Okajima K, Barrios B, Song CW (1996) Mild temperature hyperthermia combined with carbogen breathing increases tumor partial pressure of oxygen (pO_2) and radiosensitivity. *Cancer Res,* ***56(24):*** *5590-3.*
54. Iwata K, Shakil A, Hur WJ, Makepeace CM, Griffin RJ *et al.* (1996) Tumour pO_2 can be increased markedly by mild hyperthermia. *Br J Cancer Suppl,* ***27:*** *S217-21.*
55. Song CW, Park H, Griffin RJ (2001) Improvement of tumor oxygenation by mild hyperthermia. *Radiat Res,* ***155(4):*** *515-28.*
56. Wouters BG and JM Brown (1997) Cells at Intermediate Oxygen Levels Can Be More Important Than the "Hypoxic Fraction" in Determining Tumor Response to Fractionated Radiotherapy. *Radiation Research,* ***147(5):*** *541-550.*
57. Chu KF and Dupuy DE (2014) Thermal ablation of tumours: biological mechanisms and advances in therapy. *Nat Rev Cancer,* ***14(3):*** *199-208.*